Article:
Richards, R.D. orcid.org/0000-0001-7043-8372, Bailey, N.J., Liu, Y. et al. (2 more authors) (2022) GaAsBi: from molecular beam epitaxy growth to devices. physica status solidi (b), 259 (2). 2100330. ISSN 0370-1972

https://doi.org/10.1002/pssb.202100330

GaAsBi: From Molecular Beam Epitaxy Growth to Devices

Robert D. Richards, Nicholas J. Bailey, Yuchen Liu, Thomas B. O. Rockett, Abdul R. Mohmad**

Dr. R. D. Richards, N. J. Bailey, Y. Liu, Dr. T. B. O. Rockett
Department of Electronic and Electrical Engineering, University of Sheffield, S1 3JD, UK
E-mail: R.Richards@Sheffield.ac.uk

Dr. A. R. Mohmad
Institute of Microengineering and Nanoelectronics, Universiti Kebangsaan Malaysia, 43600 Bangi, Selangor, Malaysia
E-mail: armohmad@ukm.edu.my

Keywords: dilute bismide, III-V semiconductors, molecular beam epitaxy, optoelectronic devices

GaAsBi has been researched as a candidate material for optoelectronic devices for around two decades. Bi-induced localized states induce a rapid rising of the valence band edge through a band anti-crossing interaction, which has a profound effect on the band gap and the spin orbit splitting. The band engineering possible, even with just a few percent bismuth, makes GaAsBi an attractive material for THz emitters, telecommunication lasers, and low noise photodetectors, among other devices. There has been substantial progress in some of these areas; however, progress towards many of the potential applications of GaAsBi has been hindered by device quality issues, brought about by the low substrate temperatures necessary for the growth of GaAsBi with sufficiently large Bi fractions. In this review, we present an overview of the applications for which GaAsBi has been advocated and the key results in these areas. We then explore the molecular beam epitaxy growth and post-growth processing of GaAsBi and the novel techniques that have been suggested to improve material quality.

1. Introduction

Light emitters and detectors operating at 1.31 and 1.55 μm wavelengths are essential for an optical fibre communication network due to their minimised dispersion and attenuation, respectively. Huge interest has been shown towards GaAs based semiconductors due to their direct band gap and cheaper GaAs substrate compared to InP. Various GaAs based semiconductors have been studied with a view to extend the emission wavelength, including InGaAs, dilute nitrides, dilute bismides and InAs quantum dots (QDs).[1-4] For InGaAs/GaAsP quantum wells (QW), the emission wavelength is typically limited to < 1.24 μm with a maximum indium content of 40 % to avoid the formation of dislocations.[2] The introduction of nitrogen into GaAs results in rapid band gap reduction (125 meV per %N) but at the expense of optical quality degradation due to a high density of nitrogen interstitials, ion damage and low growth temperature.[5-7] It was predicted that QDs possessed superior device performance (eg. lower lasing threshold current density, J_{th}) compared to QW and bulk devices.[4] However, some of the theoretical predictions are yet to be achieved due to growth related challenges such as obtaining a homogeneous and high density population of dots while maintaining a low density of defects.[8]

The incorporation of bismuth (Bi) into GaAs introduces many interesting properties including a large band gap reduction possible with small amount of Bi, temperature insensitive band gap, large spin-orbit splitting and high electron mobility.[9-17] Hence, GaAsBi has the potential to be used for long wavelength optoelectronic devices, solar cells, bipolar transistors and spintronic devices. The introduction of Bi into GaAs reduces the band gap by increasing the valence band maximum (VBM) as well as decreasing the conduction band minimum (CBM).[18,19] The increase of the VBM is due to the anti-crossing interaction between the valence band of GaAs and the Bi defect states and can be described by the Valence Band Anti-Crossing Model.[20] The CBM can be estimated using the virtual crystal approximation (VCA) which gives a linear reduction of 23 meV per %Bi.[1] Oe and Okamoto was the first to report

that the temperature coefficient of GaAsBi (2.4 % Bi) may be as small as 0.1 meVK^{-1} which is relatively low compared to the value of 0.56 meVK^{-1} for GaAs.[21,22] Such a temperature insensitive band gap is highly desirable and could potentially reduce the cost of active cooling in laser diodes. Later, it was reported that the temperature coefficient of GaAsBi decreases monotonically with increasing Bi concentration.[23] Besides, the exciton reduced mass and hole mobility also were reported to be dependent on the Bi concentration.[24] Furthermore, GaAsBi has a large spin-orbit splitting energy which is useful to suppress Auger recombination loss in near to mid-infrared lasers. This can be achieved when the spin-orbit splitting energy is larger than the band gap of GaAsBi for [Bi] > 11 %.[25,26] Other advantages of dilute bismides include a wider scope of band structure design and strain balancing with N to obtain a quaternary alloy of substantially lower band gap while lattice matching with GaAs.

There have been several detailed reviews of the dilute bismide material system. Ref. [14] provides a comprehensive discussion of many aspects of dilute bismide ternary and quaternary semiconductors, as well as related materials including topological insulators and optical fibres. Ref. [27] covers GaAsBi growth and the growth of other dilute Bi alloys; it also includes a discussion of the III-Bi binary compounds. Ref. [28] discusses the theory and development of GaAsBi and InGaAsBi lasers in some depth. Ref. [29] provides a framework in which to consider the growth of non-equilibrium materials like GaAsBi, and indeed uses GaAsBi as an example material system. The growth of GaAsBi nanowires is reviewed in Ref. [30].

This paper will review recent research into GaAsBi, with a specific focus on device applications and the prospects for improving the molecular beam epitaxy (MBE) and post-growth material processing techniques to improve GaAsBi devices. MBE has been chosen as it is the best technique with which to pursue the growth of high Bi content GaAsBi. This requires very low growth temperatures, which preclude the use of MOVPE—a technique which

has been shown to produce excellent material quality at relatively low Bi contents (see section 2.4).

2. Recent Progress on GaAsBi Devices

2.1. Detectors

The absorption properties of GaAsBi have been investigated by several groups as shown in **Figure 1**.[31-33] Also shown for comparison is the GaAs absorption coefficient as reported by Lush et al.[34] All of the results follow the square law of the Tauc relation,[35] indicating that GaAsBi is a direct band gap material, and that it can show good absorption properties out to ~0.5 eV.

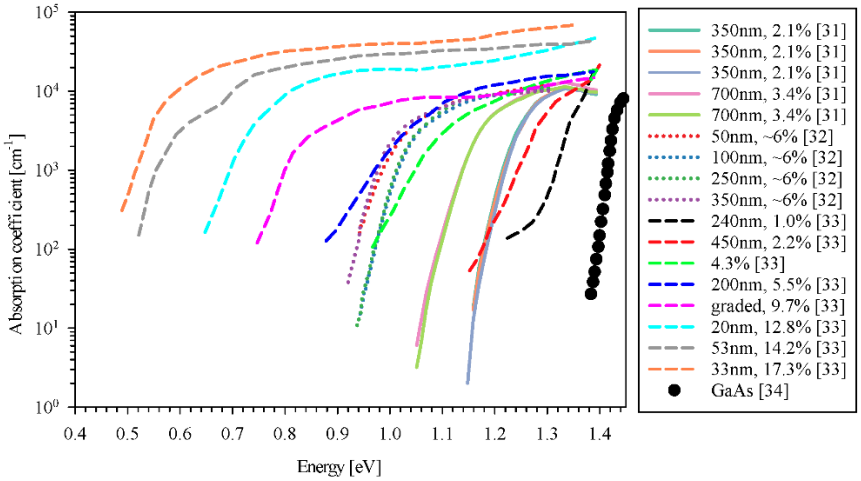

Figure 1. GaAsBi absorption coefficients reported in the literature.

The Urbach parameter is a measure of the extent of sub-band gap absorption in a material caused, in part, by crystal impurities, and has been reported for different Bi contents, as shown in **Figure 2**. Masnadi-Shirazi et al. showed that the Urbach parameter increases rapidly up to 5.5 % Bi; however, it reduces to a constant (~25 eV) at high Bi contents.[33] They suggested that this may be due to a change of shallow electronic defects near ~5 % Bi. Kakuyama et al. showed that the Urbach parameter can be affected by growth temperature, with the value for growth at 360 °C being slightly higher than that for growth at 380 °C.[36]

They attributed this to an enhanced Bi surfactant effect at the higher temperature (and Bi flux). Gogineni et al. observed temperature dependent and temperature independent components of the Urbach tail of photoluminescence (PL) spectra from a QW sample containing 5 % Bi, which they attributed to alloy fluctuations and Bi clustering respectively.[37] Clearly, the Urbach parameter is not a simple function of Bi content and likely depends on the growth conditions, which affect the behaviour of Bi on the growing surface.

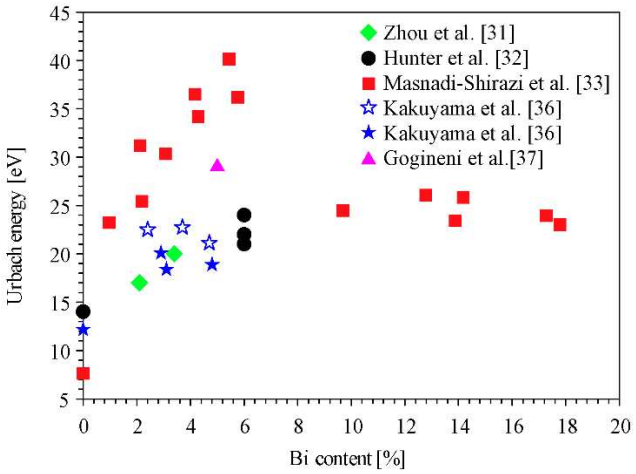

Figure 2. Urbach energy as a function of Bi content at RT from the literature. The open and solid stars represent samples grown at 360 and 380 °C, respectively.

In 2021, Liu et al. reported on the avalanche multiplication properties of a series of GaAsBi p-i-n and n-i-p diodes of various Bi contents and thicknesses.[38] They found that the enhanced spin-orbit splitting of GaAsBi prevented holes from accessing the split-off band and attaining the energies necessary to initiate impact ionisation. The result was that the hole ionisation coefficient in GaAsBi dropped dramatically with increasing Bi content, while the electron ionisation coefficient was left almost unaltered. The excess noise of an avalanche photodiode (APD) is minimised when there is a large disparity of the electron and hole ionisation coefficients and Liu et al. demonstrated that a significant reduction in noise occurred with just 4 % Bi. The addition of Bi to other alloys like InAs and AlAsSb, which already have very low noise due to their low hole ionisation coefficients,[39,40] could lead to a new family of ultra-low noise APDs.

2.2. Photovoltaics

The rapid change of band gap with Bi incorporation also lends GaAsBi to multi-junction solar cells. In a multi-junction device, several sub-cells are stacked in series in order of decreasing band gap.[41] Sub-cell band gap optimisation is crucial as the series design limits the total stack current to that of the most weakly producing layer. Metamorphic or wafer bonded architectures are used to combine mismatched materials with optimised band gaps.[42] However, to simplify production and ultimately approach the theoretical efficiency limit, the sub-cells would ideally be produced in a lattice-matched structure.

A standard 3-junction cell design employs a Ge bottom cell, InGaAs middle cell, and GaInP top cell [41], and is hindered by current under-production in the InGaAs cell. Thomas et al. predicted that efficiencies >44 % may be accessible by adding a GaAsBi-based sub-cell above the Ge sub-cell.[43] They showed that the background doping and minority carrier diffusion lengths reported for GaAsBi at the time would provide an efficiency ~42 %. Alternatively, a GaAsBi-based alloy could be the third (and forth) junction in a 3 (4)-junction cell grown on GaAs, eliminating the need for a group-IV substrate. Zayan et al. calculated the performance of a Ge cell and compared it with a 12 % GaAsBi cell of the same band gap.[44] The GaAsBi produced a higher open circuit voltage (V_{OC}), at the expense of a reduced short circuit current (I_{SC}). The result suggests that GaAsBi may make an effective bottom cell.

Several groups have reported experimental results from GaAsBi-based cells.[45-48] Some focused on multiple quantum well (MQW) designs, which are advantageous because they can decouple the absorption edge and average lattice constant.[49] Richards et al. reported a series of GaAsBi/GaAs MQW diodes containing between 3 and 63 QWs.[45] As shown in **Figure 3**, the V_{OC} was ~0.45 V which is relatively low for an absorption edge of ~1.1 eV. They attributed this to trapping of holes in the QWs.[50] Strain relaxation prevented them from investigating the

higher numbers of QWs necessary for high efficiency. In 2018, Kim et al. addressed this issue with a 50-period, strain-balanced GaAsBi/GaAsP cell (grown by metal-organic vapour phase epitaxy).[46] They showed an improved V_{OC} of 0.75 V. However, their I_{SC} was limited to 13.6 $mAcm^{-2}$, probably due to the presence of carbon background doping.

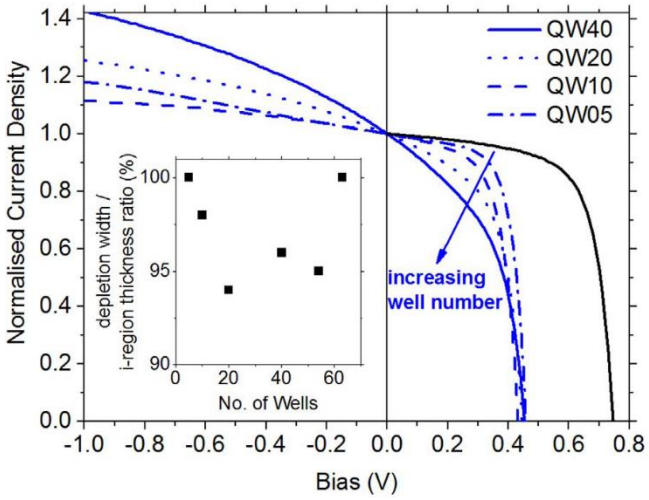

Figure 3. Illuminated current density curves from a series of GaAsBi/GaAs MQW devices, compared with an InGaAs/GaAsP MQW (solid black line). The GaAsBi devices were illuminated with the AM1.5 spectrum truncated at 900 nm to simulate operation under an InGaAs subcell. Reproduced with permission.[45] Copyright 2017, Elsevier.

Hasegawa et al. investigated bulk GaAsBi cells.[48] They found a roughly linear reduction of V_{OC} with increasing Bi composition from 0.7 V at 0 % to ~0.3 V at 8.4 % Bi. These values are relatively low, but the consistency with their GaAs result suggests that the presence of Bi is not limiting the V_{OC} (the world record GaAs cell has a V_{OC} of ~1.13 V [42]). Muhammetgulyyev et al. have also presented a GaAsBi-based bulk solar cell.[47] They found a comparable V_{OC} to Richards et al. and Hasegawa et al., at 0.47 V, which they attributed to the formation of a Schottky junction between the p-GaAs and the GaAsBi i-region, caused by the formation of metallic Bi clusters. Ultimately, it is probably necessary to strain-balance a GaAsBi-based solar cell, potentially with a similar design to the 2011 world record cell,[51] which contained an InGaAsN layer, for example by using GaAsBiN.[52]

2.3. Light Emitting Diodes (LEDs)

GaAsBi based LEDs emitting at 1300 and 1550 nm are of interest for telecommunications while 1000–1050 nm wavelengths are applicable to optical coherence tomography due to the large electroluminescence (EL) full width at half maximum (FWHM) caused by the bismuth-induced localised states. Lewis et al. showed the first RT EL at 987 nm from a 50 nm, GaAsBi ([Bi] = 1.8 %) active region (see **Figure 4**).[53] The peak wavelength was unchanged in the temperature range 100–300 K and it had a large spectral width of 143 meV. EL was shown in the current density range 50–100 Acm^{-2}. A difference in the PL and EL peak wavelengths was attributed to electrically injected holes occupying deeper trap levels than the more energetic holes created by optical injection.

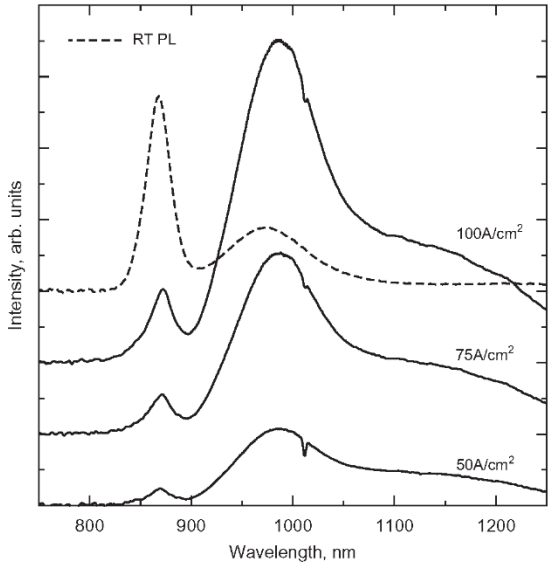

Figure 4. RT EL spectra from a GaAsBi LED at different injection currents. A RT PL spectrum is also included for comparison. Reproduced with permission. [53] Copyright 2009, Elsevier.

Richards et al. demonstrated GaAsBi ([Bi] = 6 %) LEDs with 50 nm active region emitting at ~1200 nm at RT, with a FWHM of 117 meV in the current density range 8–80 Acm^{-2}.[54] Current dependent integrated EL measurements showed that radiative and non-

radiative recombination mechanisms dominated at 20 K and RT, respectively. A temperature dependent analysis of the integrated EL highlighted a continuous distribution of Bi-induced localised states extending up to 75 meV into the band gap. Patil et al. grew an 11-period, GaAsBi ([Bi] = 4 %) MQW LED.[55] The wells and barriers were grown at 350 and 550 °C, respectively, aiming to reduce Bi segregation. EL spectra at 76–1000 Acm^{-2} yielded a peak at 1230 nm and FWHM of 100 meV at RT. A super-linear dependence of the light output with injection current was observed. Meanwhile, Hossain et al. studied the pressure and temperature dependence of a GaAsBi/GaAs LED containing a 50 nm, GaAsBi ([Bi] = 1.4 %) layer.[56] The peak was at 936 nm at 260 K with an FWHM of 62 meV. The authors concluded that the GaAsBi/GaAs interface has a type-I band alignment based on high pressure EL measurements, and that a rapid decrease in EL intensity at higher temperatures implies that non-radiative recombination becomes dominant.

2.4. Lasers

A detailed discussion of the physics of dilute bismide lasers is available elsewhere.[28] The key development since that publication has been a new GaAsBi lasing wavelength record set by an optically-pumped microdisk GaAsBi laser.[57] It can be seen from **Table 1** that MOVPE can produce lasers with lower threshold current densities than are achievable with MBE. However, at growth temperatures significantly below 400 °C, as required for Bi fractions greater than ~4 % (see **Figure 7**), the surface chemical reactions necessary for MOVPE to proceed are unable to occur. For the larger Bi fractions necessary to target telecoms wavelengths, MBE must be utilised, or the development must be moved to a different platform, such as InP.[28]

The advantage of GaAsBi due to the suppression of CHSH Auger recombination is even more profound for laser diodes. However, the laser results to date have not reached the necessary ~11 % Bi. The first optically-pumped GaAsBi laser was demonstrated by Tominaga

et al. in 2010.[58] The device contained a 390 nm GaAsBi ([Bi] = 2.5 %) layer, grown at 350 °C by MBE. The laser operated at RT at 982.8 nm. From 160 to 240 K, the emission energy decreased at a rate of 0.18 meVK^{-1} which is ~40 % of the rate for GaAs. The threshold pumping density was linear with increasing temperature up to 240 K, at which point it dramatically increased and the emission energy blueshifted. This was attributed to the material's band offsets, where there is a large offset of the valence band and relatively small offset of the conduction band. In 2013, the same group improved their GaAsBi laser diode design.[59] Prior to the growth of a GaAsBi ([Bi] = 5.8 %) active layer, an AlGaAs electron-blocking layer was grown. The peak emission was at 1204 nm at RT. Over the temperature range 20 to 80 °C, the peak wavelength temperature coefficient was roughly 40 % of that of a 1300 nm GaInAsP laser.

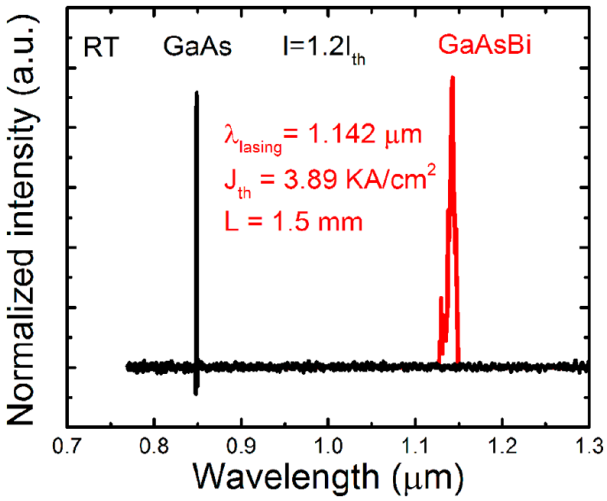

Figure 5. Lasing spectra of electrically pumped GaAs and GaAsBi lasers. Reproduced with permission. [60] Copyright 2017, American Chemical Society.

The first electrically pumped GaAsBi single QW laser was reported by Ludewig et al. in 2013.[61] A 6.4 nm GaAsBi ([Bi] = 2.2 %) layer was embedded between two 150 nm AlGaAs ([Al] = 20 %) barriers, further sandwiched between two 1.4 μm AlGaAs ([Al] = 40 %) n- and p-doped layers. The J_{th} was around 1.56 kAcm^{-2} with emission at 947 nm at RT. In 2014, Fuyuki et al. reported similar devices incorporating 3 % and 4 % Bi content, emitting at up to

1045 nm at RT.[62] The temperature coefficient of the 3 % Bi content laser was 0.17 nmK^{-1}, consistent with their previously reported, optically pumped laser.[59] Butkute et al. demonstrated a three-period, 8 nm QW GaAsBi/GaAs laser ([Bi] > 6 %).[63] The structure was grown by a combined MOVPE/MBE growth approach, with the QW region grown using MBE and the rest of the structure grown by MOVPE. Lasing measurements showed a pronounced narrow spectrum at 1060 nm. In 2017, Wu et al. reported an electrically pumped GaAsBi ([Bi] = 5.8 %) laser grown by MBE, as shown in **Figure 5**.[60] The lasing wavelength was 1135 nm at 273 K under CW operation and 1142 nm at up to 350 K in pulsed mode. In 2019, the low-frequency of noise characteristics of GaAsBi ([Bi] = 8 %) were investigated by Glemža et al.[64] To date, the longest optically pumped lasing wavelength is 1407 nm, reported by Liu et al. in 2019, with a 5.8 % Bi content.[57] This laser used a microdisk structure, which has great potential for application in modern photonic integration compared to the Fabry-Perot-based design. The properties of GaAsBi laser are summarized in Table 1. More recent work has advocated the use of GaAsBi quantum dots in a GaSb host matrix to exploit the advantages of GaAsBi for laser design, while minimising the Bi content required to reach long wavelengths.[65,66] This work is potentially very interesting, but beyond the scope of this review.

Table 1. GaAsBi laser characteristics reported in the literature.

Author, Year, reference	Theoretical or experimental and growth process	Structure	Bi content [%]	Lasing wavelength [nm]	Pumping density/ threshold current density at RT
Tominaga, 2010, [58]	MBE	Bulk	2.5	982.8, 986.2	2.5 mJ/cm^2
Fuyuki, 2013, [59]	MBE	Bulk	4.2	1088.6, 1204	0.36 mJ/cm^2
Ludewig, 2013, [61]	MOVPE	QW	2.2	947	1.56 kA/cm^2

Fuyuki, 2014, [62]	MBE	Bulk	3, 4	976, 1045	15, 8 kA/cm^2
Marko, 2014, [67]	MOVPE	QW	4.4	1038	4.5 kA/cm^2 at 180K
Butkute, 2014, [63]	Hybrid MBE/MOVPE	QW	~ 6.5	1060	30 kA/cm^2
Broderick, 2015, [68]	Theoretical	QW	13	1550	-
Wu, 2017, [60]	MBE	QW	5.8	1135, 1142	5.2 kA/cm^2 at 273K 3.89 kA/cm^2
Glemža, 2019, [64]	MBE	QW	8	1090	-
Liu, 2019, [57]	MBE	QW	5.8	1276, 1407	21 µW (per micro-disk)

2.5. THz

THz signal generation is challenging as microwave transmitters struggle to reach such short wavelengths, [69] and the photon energy is similar to kT at RT, ruling out semiconductor band to band transitions. THz radiation is routinely produced using transient photocurrents and photoconductive antenna (PCA), [70] although there are other alternatives (see [71] for a more complete description, and [72,73] for the THz generation mechanisms present in GaAsBi). Illuminating a semiconductor material between two biased electrodes with an ultra-short pulse produces a short-lived transient photocurrent. If the photocurrent transient is sufficiently short, then its Fourier transform will contain a substantial bandwidth of components in the THz regime.[74]

An effective PCA material will be highly resistive in the dark to reduce heating, have a large breakdown voltage to enable a large bias, a reasonable carrier mobility to enable high currents and a very short carrier lifetime.[74]. The last point is critical as a shorter pulse will have components covering a larger THz spectral bandwidth. Low-temperature-grown GaAs (LT-GaAs) is a common active material in PCAs, with a short (< 1 ps) carrier lifetime and high resistivity;[75] however, its absorption wavelength is effectively fixed ~900 nm, preventing its use with cheap, compact, longer-wavelength, fibre-coupled lasers.[71] GaAsBi can overcome

the wavelength limitation of LT-GaAs, without the increase in carrier lifetime and decrease in conductivity observed in InGaAs.[76]

In 2006, Bertulis et al. reported the growth of two 500 nm GaAsBi layers at 280 and 330 °C.[77] The 280 °C sample absorbed up to 1.4 µm, had a lifetime of ~1 ps, a resistivity > 60 Ωcm, and a bandwidth of 3 THz. They attributed the high resistivity to As antisites. Similar layers have been shown to produce THz radiation with a similar bandwidth when excited by longer wavelength sources,[78-80] including in the telecommunication C band.[81,82] In 2013, Heshmat et al. benchmarked a GaAsBi-based THz system against a commercially available LT-GaAs system and showed that it exhibited a larger bandwidth and a higher efficiency. [83] GaAsBi based PCAs are now commercially available.[74] A representative THz power spectrum is shown in **Figure 6**.[78]

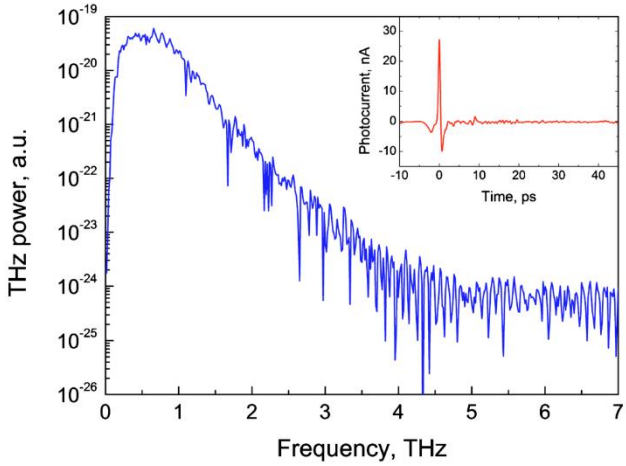

Figure 6. Fourier spectrum of a THz radiation transient. The bandwidth is ~4 THz and the signal to noise ratio is ~50 dB. The inset shows the corresponding photocurrent transient, generated using a 70 fs laser pulse at 1030 nm. Reproduced with permission. [78] Copyright 2010, American Institute of Physics.

2.6. Spintronics

To assess the potential of a particular material system for spintronic, two important parameters are typically assessed which are g-factor and electron spin relaxation time (τ_s). The g-factor describes the response of the electron spins to externally applied magnetic field while the τ_s

must be longer than the manipulation time to be able to utilize electron spins as an information vector.[84,85] In 2006, Fluegel et al. proposed the possibility of Bi alloying as a means to manipulate the spin orbit gap of GaAsBi for spintronic application.[12] This is based on the giant spin-orbit splitting energy observed in GaAsBi with the incorporation of Bi. The modulation of band gap and spin-orbit splitting due to Bi incorporation influences the spin relaxation. According to the theoretical study reported by Tong et al., the τ_s decreases dramatically with the increase of Bi concentration (up to 10% Bi).[86] For intrinsic GaAsBi, the τ_s is dominated by the Dyakonov-Perel (DP) mechanism due to short relaxation time. At 300 K, the DP electron spin relaxation time is at least 40 times smaller than the Bir-Aronov-Pikus (BAP) electron spin relaxation time.

In 2013, Pursley et al. carried out Hanle effect measurements on 100 nm thick GaAsBi (0.8% Bi) to estimate the product of the g-factor and the spin relaxation time ($g.\tau_s$).[87] In Hanle measurements, the g-factor and the τ_s cannot be uncoupled. It was found that the product of $g.\tau_s$ ranges from 0.8 nm at 40 K and 0.1 ns at 120 K. Later, Mazzucato et al. reported the g-factor and the τ_s of GaAsBi independently by carrying out time-resolved PL measurements.[88] The measurements were carried out at temperatures >100 K to avoid localization effects. It was found that the g-factor increases from -0.81 to -0.68 for temperatures between 100 and 300 K, respectively. This value is twice compared to the g-factor of GaAs which is -0.41 at 100 K. Furthermore, the τ_s decreases from 370 to 100 ps when the temperature increases from 100 to 300 K. The product of $g.\tau_s$ obtained by Mazzucato et al. is consistent with the earlier report by Pursley et al. measured by Hanle effect measurements. Recently, electron spin dynamics of GaAsBi bulk (1-3.8% Bi) and quantum wells (2.4-7% Bi) were studied by Azaizia et al.[85] For both structures, a clear decrease of τ_s with the increase of Bi concentration were observed. These are also attributed to increased efficiency of the DP mechanism due to stronger spin-orbit interaction.

3. Prospects for Improving MBE Growth

Further developments in GaAsBi device applications will be enabled by refinement of the material properties. There are two approaches to this: (i) improve the growth of the material and (ii) formulate post-growth processing. Here we will discuss reports of GaAsBi growth and prospects for new growth techniques, and also the use of thermal annealing and passivation post-growth. We will start with a review of the influence of key MBE growth parameters on the incorporation of Bi into GaAs.

3.1. Substrate Temperature

At typical GaAs growth temperatures (~580 °C) Bi can only be used as a surfactant as it will segregate rather than incorporate at this temperature.[89] For GaAsBi growth, the substrate temperature must be reduced to ≤ 420 °C,[90] to improve the low solubility of Bi within GaAs and to give Ga-Bi bonds a sufficient lifetime for Bi to be incorporated. Figure 7 shows a mapping of the reported substrate temperatures and epilayer Bi contents from the literature.[1,10,36,37,91-105] Most of the growth effort has been concentrated on relatively low (< 10 %) Bi contents and relatively high (> 300 °C) growth temperatures, although some groups have targeted lower growth temperatures and higher Bi contents. The hashed area in figure 7 is not a theoretical limit, rather it is simply a guide to the eye. As discussed in section 3.5, the growth of GaAsBi with a Bi flux substantially higher than the Bi incorporation rate results in excess Bi accumulating on the growing surface, which represents un-incorporated Bi and can actually act to reduce the effective Bi flux by forming droplets that remove individual Bi atoms from the surface. While it is not a hard limit on the Bi incorporation achievable at each temperature, the hashed region in Figure 1 has, to date, proven inaccessible.

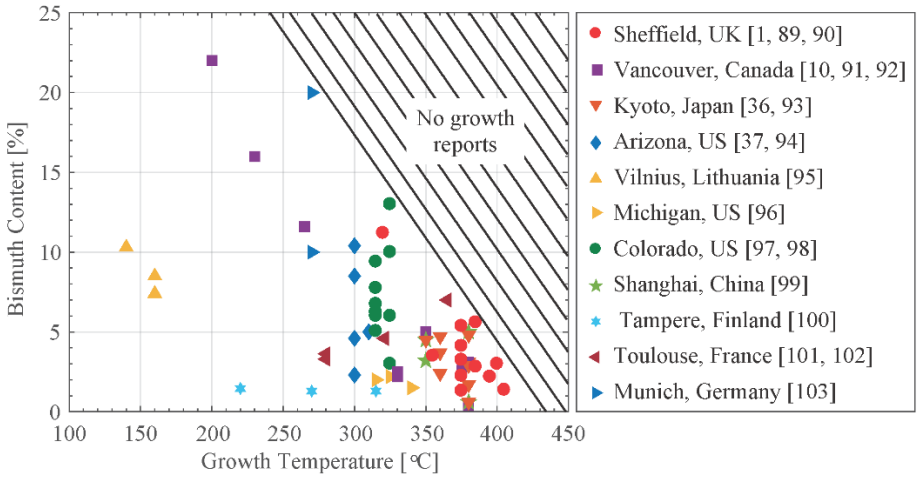

Figure 7. Bi contents reported at different MBE growth temperatures, arranged by institute of origin.

3.2. Material Flux Ratios

As tends to compete with Bi for group V lattice sites,[94] meaning a near stoichiometric As:Ga flux ratio is essential for Bi incorporation.[90,94,106,107] A stoichiometric flux can also reduce the density of the As antisite defects abundant in LT-GaAs.[108] Sufficiently high As overpressures can cause the formation of Bi droplets as discussed in section 3.5. While the As species used appears to have negligible effect on the material properties, it has been observed that Bi incorporation is slightly more favourable under As_4 than As_2.[90,109]

For growth well below the thermal Bi limit indicated in Figure 7—the "kinetically limited regime" —the Bi content is essentially flux limited and can therefore be controlled by the Bi cell temperature.[99] To produce high quality material for optoelectronic devices, it has been shown that higher growth temperatures are required.[36,91] Therefore, the Bi flux should be increased to the near the thermal limit, just before the regime where segregated Bi forms droplets (see section 3.5). At low densities, this Bi coverage acts as a surfactant and can improve crystal quality,[99] but past a critical density this forms metallic droplets of Bi on the surface, reducing layer uniformity and affecting the optical properties.[110]

The Ga:Bi flux ratio is more complex. At lower growth temperatures the Bi content appears to be linear with respect to Bi flux and therefore to Ga:Bi.[105] At higher temperatures

Bi desorption from the surface becomes significant and the low solubility of Bi in GaAs is seen in the much reduced maximum Bi contents shown in Figure 7. It is important to note that the Bi flux will also impact the surface reconstruction during growth and that this will affect how Bi incorporates.

3.3. Surface Reconstruction

Whilst the surface reconstruction during growth is determined by the material flux ratios and growth temperature which individually impact on GaAsBi growth, it is useful to understand how the reconstruction itself impacts Bi incorporation. Indeed, it has been shown that the (2 × 1) reconstruction impacts on Bi clustering in this material.[111] Norman et al. also postulated that the disappearance of this reconstruction may be linked to the onset of phase separation in higher Bi content layers.[100] A recent growth study by Cornille et al. used substrate curvature measurements to calculate the Bi content during growth.[103] Comparing the reflected high energy electron diffraction pattern and stress profiles, they found that the Bi incorporation efficiency was high under a (1 × 3) reconstruction, then reduced as the reconstruction transitioned to (2 × 1), as illustrated in **Figure 8**. Similar Bi content profiles have been observed elsewhere and may also be related to reconstruction transitions.[112] Further work is required to fully understand the role of reconstruction in Bi incorporation. Of particular interest is how an increased Bi flux would affect the relative incorporation under the (1 × 3) and (2 × 1) reconstructions, as the Bi contents reported in [103] are somewhat lower than the highest Bi contents reported at that growth temperature.

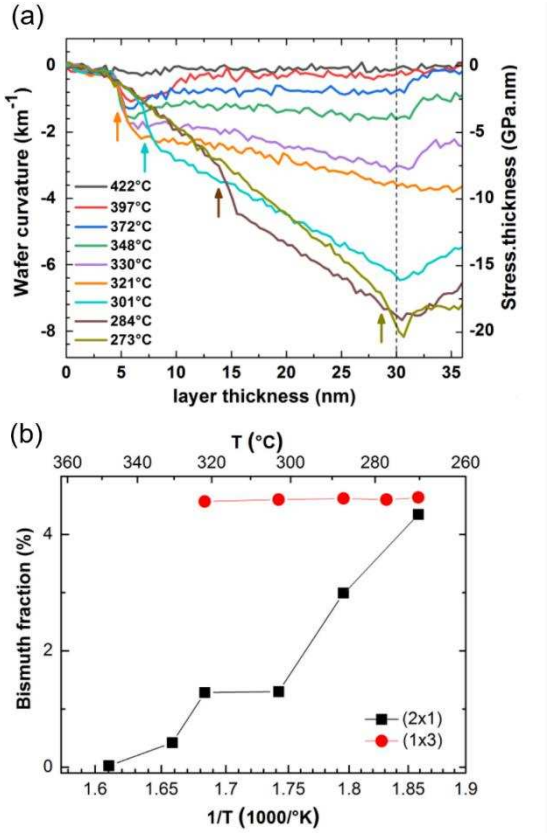

Figure 8. a) Curvature evolution during GaAsBi growth (a steeper gradient corresponds to more Bi incorporation) and b) rate of Bi incorporation with respect to growth temperature. Reproduced with permission.[103] Copyright 2019, American Institute of Physics.

3.4. Growth Rate

The impact of growth rate on the quality of GaAsBi has not been fully investigated. Ptak et al. studied the impact of growth rate on Bi incorporation and surface roughness at the growth temperature of 315 °C.[99] All of the samples were grown in the kinetically limited regime—the Bi content appeared to be proportional to the Bi flux and was well-below the ~14 % predicted to be possible at that temperature in Figure 7. At lower growth rates, droplets were observed at high Bi:Ga flux ratios. This was attributed to the increased monolayer growth time allowing for more Bi to segregate to the surface. On the other hand, higher growth rates exhibited higher surface roughness at the lower Bi contents, which was attributed to a reduced Bi surface coverage and surfactant effect. The findings of this work were contrasted by Lu et al., who presented that low growth rates are key to reducing Bi droplet density.[106]

3.5. Bi on a Growing Surface

The incorporation of Bi into GaAs appears to proceed via an intermediate state, wherein the Bi is physisorbed on the growing surface, prior to incorporating. While the detailed mechanisms are not clearly established, it is useful to explore the available information on this process. Again, this section will focus on the reports of MBE, although there are many parallels with MOVPE growth.

While it is possible to produce high quality GaAsBi with a) no surface-droplets, it is reasonably common to see b) Bi, c) Ga or d) Ga-Bi droplets on the surface post-growth. The regimes in which these four conditions are observed (at a growth temperature of 325 °C) are shown in **Figure 9**.[113] A V:III atomic flux ratio < 1 promotes Ga droplets due to the low rate of surface Ga desorption.[94,106,107,114] Bi droplets are observed when the rate of Bi deposition exceeds the sum of the Bi incorporation and desorption rates.[106,107] High temperature and high As flux both limit the Bi incorporation rate, while high growth rates incorporate Bi from the surface more rapidly for a given incorporation efficiency.[99] The Bi desorption rate is a function of temperature and surface Bi coverage.[115] Bi droplet formation can also be precipitated by Ga droplet formation.[113]

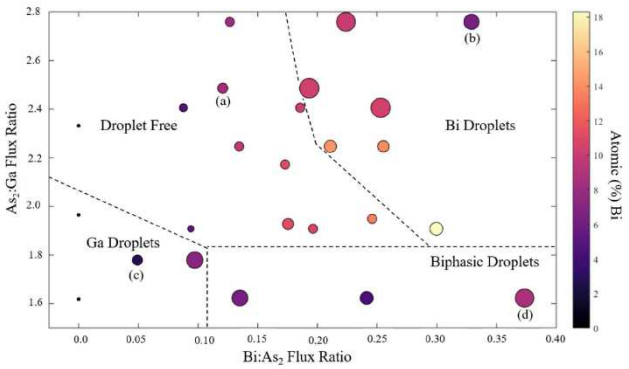

Figure 9. The growth parameters under which surface droplets are observed at 325 °C. The data point size represents the broadness of the XRD GaAsBi peak. Reproduced with permission.[113] Copyright 2020, Elsevier.

The highest Bi incorporation efficiencies are found near the onset of Bi droplets,[113] which is unsurprising as the Bi droplets act to remove Bi from the surface.[98,110,113,116-120] Due

to the mobility of Bi droplets, they can give rise to Bi-poor nano-structures within the GaAsBi matrix.[98] Ga droplets, on the other hand, appear to promote Bi incorporation via a vapour-liquid-solid mechanism (see the pulsed growth section).

As droplets form due to Bi and/or Ga accumulation on the growing surface, they can nucleate tens or even hundreds of nm after the start of growth. This has implications for simultaneously maximising the Bi content and the growth temperature, as required for the best device properties [121]. Maximal Bi content requires growth on the cusp of Bi droplet formation; however, for thicker devices, it is necessary to reduce the Bi flux and temperature in order to remain droplet-free. It may be possible to use growth halts to crystallise excess Ga and desorb excess Bi.[120] However, growth interrupts, and even GaAs overgrowth cannot remove all of the surface Bi.[122,123] Post-growth removal of Ga droplets does not mitigate the compositional inhomogeneity formed during growth.[118]

3.6. Pulsed Growth

In 2015, Wood et al. showed that oscillating flux ratios can produce enhanced Bi contents.[124] They attributed this to a periodic accumulation and crystallisation of surface Ga droplets and a resulting vapour-liquid-solid incorporation pathway. This study was performed at 320 °C and observed average Bi contents of ~ 3 %—far lower than the limit imposed by the growth temperature (see Figure 7). Stevens et al. made similar observations at 250 °C.[125] However, it is not yet clear whether this technique can increase the Bi contents accessible at high temperatures, as required for high quality device growth. Existing temperature-limited Bi content predictions are all based on quasi equilibrium growth conditions [94,99,106] and exceeding these limits through non-equilibrium growth may lead to substantially reduced device dark currents.[121]

4. Post-Growth Processing

4.1. Thermal Annealing

Since GaAsBi requires a relatively low growth temperature, thermal annealing is expected to improve the wafer quality as well as device performance. For GaAsBi, thermal annealing typically led to a modest PL intensity improvement of ~1.3 to 3 times and FWHM reduction of ~10–20 % while the peak energy remained unchanged or showed a small blueshift (~5–15 meV), as shown in **Figure 10** (a).[104,126-129] Besides, the carrier decay time of annealed GaAsBi increases from 130 to 180 ps at RT.[128] These results indicate that GaAsBi is thermally stable, and annealing is useful in reducing the density of non-radiative defects.

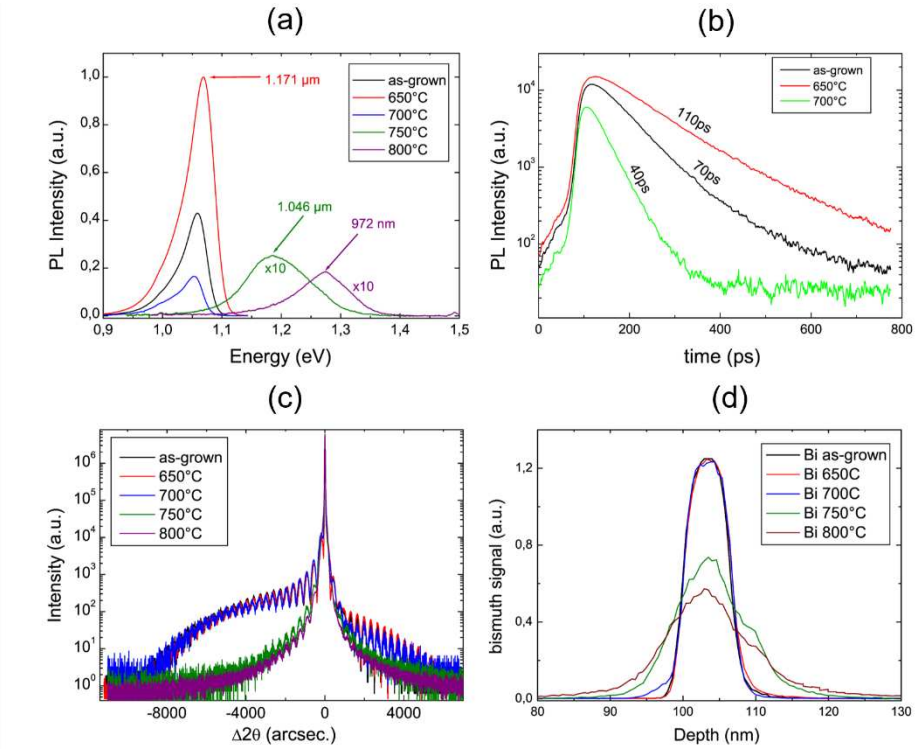

Figure 10. Optical and structural properties of an as-grown and annealed GaAsBi QW. The annealed temperature is between 650 and 800 °C for 30 seconds. (a) 20 K PL spectra and (b) RT time-resolved PL showing carrier decay time. (c) The (004) HR-XRD ω-2θ spectra and (d) Bi SIMS profiles showing Bi out-diffusion for annealing temperatures ≥ 750 °C. Reproduced under terms of the CC-BY license.[104] Copyright 2014, The authors, published by Springer Nature.

The optimum annealing temperature is typically between 500 and 700 °C depending on: (i) Bi concentration, and (ii) thickness of the bismide layer. According to Mohmad et al.,

the optimum rapid thermal annealing (RTA) temperature is 700 °C for 30 seconds for [Bi] < 4.8 % but reduces to 600 °C for higher concentrations.[129] A similar trend was also observed in dilute nitride, i.e GaNAs in which the optimum annealing temperature reduces from 1000 to 700 °C when the N concentration increases from 0.06 to 6 %.[130,131] Besides, the optimum annealing temperature depends on the thickness of the GaAsBi layer. A thin bismide layer or a QW structure requires a lower annealing temperature compared to a thicker one. For a ~7 nm GaAsBi single QW, regardless of the Bi concentration, the optimum annealing temperature is < 650 °C.[104,126] However, for a 200 nm GaAsBi ([Bi] = 2.3%) layer, the optimum annealing temperature was reported to be as high as 750 °C for 30 seconds.[128]

Based on Ref. [129], thermal annealing does not necessarily reduce the localization effects or the so-called S-shape behaviour in GaAsBi which is typically associated with alloy fluctuations and Bi clustering. Samples which showed identical S-shape behaviour between the as-grown and the annealed one may also show similar PL intensity improvement. Hence, it is likely that the modest PL improvement obtained by annealing is dominated by the removal of Ga or As related defects induced by the low growth temperature, and not the removal of Bi related defects.

Most of the previous studies reported that QW and thin GaAsBi layers are stable at temperatures < 750 °C.[104,126,129] For higher temperatures, significant Bi out-diffusion will occur to the adjacent GaAs barriers, as shown by the Bi SIMS profile in Figure 10(d). This was also accompanied by a significant PL peak blueshift (> 120 meV) and PL intensity degradation.[104] It is important to note that the material that forms the barriers plays an important role in determining the Bi out-diffusion. Unlike GaAsBi/GaAs, GaAsBi QWs with AlAs barriers have been shown to prevent Bi out-diffusion.[132,133] As a result, the Bi that migrated during the annealing process coalesced to form Bi nanocrystals or dots inside the GaAsBi well.[132,133] Reports on the effect of annealing on device performance is currently

limited. Recently, Kim et al. reported that in-situ annealing at 630 °C for 30 minutes increases PL intensity as well as reduces the J_{th} of a bismide laser from 6 to 5.25 $kAcm^{-2}$.[127]

4.2. Passivation

Passivation is commonly used in the semiconductor industry to reduce carrier trap density to improve optical and electrical performance of devices. For example, hydrogen passivation by exposing a GaAs crystal to hydrogen plasma is known to be effective in rendering the deep level defect at 0.82 eV below the CBM electronically inert.[134] This is attributed to the interaction between the hydrogen and the unsaturated bond of the As antisite (As_{Ga}) defect which led to the formation of stable As-H bonds.

Post-growth hydrogenation of GaAsBi with a wide range of Bi concentrations ($0.6 \leq [Bi] \leq 10.6$ %) was carried out by Pettinari et al.[135] It was found that hydrogenation passivates the Bi-induced shallow acceptor level (E_a ~ 27 meV) which is responsible for p-type conductivity in undoped GaAsBi. As a result, the hole density of hydrogenated bismide reduces from 10^{17} to 10^{15} cm^{-3} while the hole conductivity increases tenfold, as shown in **Figure 11**. However, hydrogenation did not fully passivate deep Bi-acceptor levels with E_a ~ 278 meV. The shallow and deep acceptor states were attributed to small Bi clusters (consisting of two to three Bi atoms) and big Bi clusters, respectively. In addition, the PL emission energy remained the same after hydrogenation, suggesting that hydrogen passivation did not influence the GaAsBi band gap.

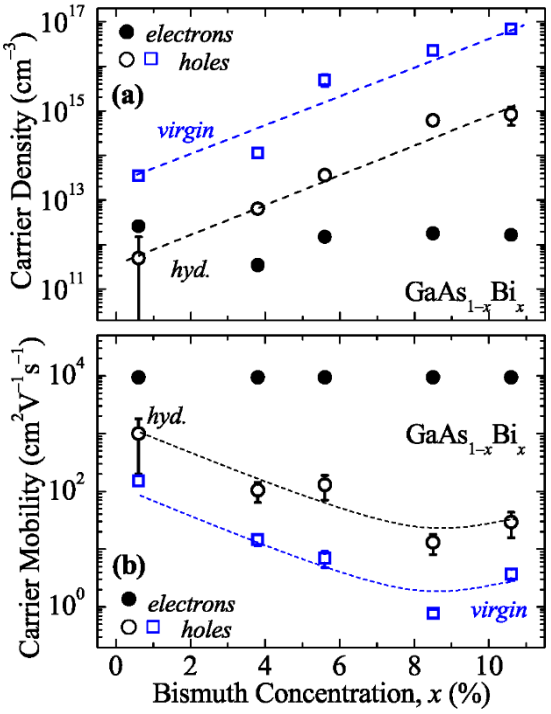

Figure 11. The dependence of (a) carrier density and (b) carrier mobility on Bi concentration for as-grown and hydrogenated GaAsBi. Hydrogenation reduces hole density and improves hole mobility. The dashed lines are guides to the eye. Reproduced with permission.[135] Copyright 2012, American Institute of Physics.

Based on a first-principles study reported by Luo et al., hydrogen passivation is effective in passivating Ga vacancy (V_{Ga}) defects which are a dominant defect in n-type GaAsBi.[136] The formation of V_{Ga}+nH (where $1 \leq n \leq 4$) removed all defect levels induced by V_{Ga} from three to zero. However, hydrogen passivation did not remove the deep level defect located at 0.33 eV above the VBM induced by Bi_{Ga}, consistent with observation reported by Pettinari et al. [135]. Besides, facet passivation may reduce low frequency noise of GaAsBi laser diodes due to surface leakage.[64] Sulfur passivation treatment on the facet surface has been shown to reduce surface states in GaAs laser diodes, increase the threshold for the onset of catastrophic optical degradation (COD) in InGaAs and AlGaInP laser diodes and improve the reliability of InGaAsP laser diodes.[137-140] To date, the effect of sulfur passivation on the facet surface of GaAsBi laser diodes has not been reported.

5. Summary and Outlook

Throughout this paper we have discussed many of the applications for which GaAsBi has been identified as a promising candidate. The powerful band engineering enabled by even small fractions of Bi has already been demonstrated to be advantageous for devices—low-noise avalanche photodiodes can be designed by manipulating the spin-orbit splitting; THz emitters can be adapted for longer wavelength excitation by manipulating the band gap. For applications requiring larger Bi fractions, e.g. lasers with suppressed Auger recombination, further development of growth and post-growth-processing techniques is required.

The interplay of Bi and Ga droplets on the growing GaAsBi surface is complex, and control of that interplay is essential to maintain a partially Bi-covered surface and maximise the beneficial Bi surfactant effect. It is also necessary to more deeply understand the mechanism by which Bi incorporates into the growing film, as dynamic, reconstruction- or droplet-mediated incorporation mechanisms may be capable of producing higher Bi contents at higher temperatures than have been accessible to date.

Acknowledgements

The work of RDR was funded by the Royal Academy of Engineering under the Research Fellowships scheme. The Engineering and Physical Sciences Research Council funded the work of TBOR (EP/S036792/1) and NJB (Doctoral Training Program). The work of ARM was funded by the Malaysia Ministry of Higher Education through Fundamental Research Grant Scheme (FRGS/1/2019/STG07/UKM/02/6). RDR would like to thank Mr Matthew Carr and Professor John David for useful discussions.

Received: ((will be filled in by the editorial staff))
Revised: ((will be filled in by the editorial staff))
Published online: ((will be filled in by the editorial staff))

References

[1] A. R. Mohmad, F. Bastiman, C. J. Hunter, R. D. Richards, S. J. Sweeney, J. S. Ng, J. P. R. David, B. Y. Majlis, *Phys. Status Solidi B* **2014**, *251*, 1276
[2] N. Tansu, J.-Y. Yeh, L. J. Mawst, *IEEE J. Sel. Top. Quantum Electron.* **2003**, *9*, 1220
[3] J. S. Harris, *Semicond. Sci. Technol.* **2002**, *17*, 880
[4] M. Asada, Y. Miyamoto, Y. Suematsu, *IEEE J. Quantum Electron.* **1986**, *22*, 1915

[5] S. Wang, Y. Q. Wei, X. D. Wang, Q. Zhao, M. Sadeghi, A. Larsson, *J. Cryst. Growth* **2005**, *278*, 734
[6] S. G. Spruytte, C. W. Coldren, J. S. Harris, W. Wampler, P. Krispin, K. Ploog, M. C. Larson, *J. Appl. Phys.* **2001**, *89*, 4401
[7] J. Gupta, G. Sproule, X. Wu, Z. Wasilewski, *J. Cryst. Growth* **2006**, *291*, 86
[8] M. Maximov, V. Ustinov, A. Zhukov, N. Kryzhanovskaya, A. Payusov, I. Novikov, N. Y. Gordeev, Y. M. Shernyakov, I. Krestnikov, D. Livshits, *Semicond. Sci. Technol.* **2008**, *23*, 105004
[9] S. Francoeur, M. J. Seong, A. Mascarenhas, S. Tixier, M. Adamcyk, T. Tiedje, *Appl. Phys. Lett.* **2003**, *82*, 3874
[10] S. Tixier, M. Adamcyk, T. Tiedje, S. Francoeur, A. Mascarenhas, P. Wei, F. Schiettekatte, *Appl. Phys. Lett.* **2003**, *82*, 2245
[11] W. Huang, K. Oe, G. Feng, M. Yoshimoto, *J. Appl. Phys.* **2005**, *98*, 053505
[12] B. Fluegel, S. Francoeur, A. Mascarenhas, S. Tixier, E. C. Young, T. Tiedje, *Phys. Rev. Lett.* **2006**, *97*, 067205
[13] A. Mascarenhas, Y. Zhang, J. Verley, M. J. Seong, *Superlattices Microstruct.* **2001**, *29*, 395
[14] S. Wang, P. Lu, *Bismuth-Containing Alloys and Nanostructures*, Springer, Singapore **2019**
[15] T. Tiedje, E. C. Young, A. Mascarenhas, *International Journal of Nanotechnology* **2008**, *5*, 963
[16] B. Zhang, W.-Y. Qiu, P.-P. Chen, X.-J. Wang, *J. Appl. Phys.* **2018**, *123*, 035702
[17] M. Mbarki, A. Rebey, *Semicond. Sci. Technol.* **2011**, *26*, 105020
[18] G. Pettinari, A. Polimeni, M. Capizzi, J. H. Blokland, P. C. M. Christianen, J. C. Maan, E. C. Young, T. Tiedje, *Appl. Phys. Lett.* **2008**, *92*, 262105
[19] G. Pettinari, O. Drachenko, R. Lewis, T. Tiedje, *Phys. Rev. B* **2016**, *94*, 235204
[20] K. Alberi, O. D. Dubon, W. Walukiewicz, K. M. Yu, K. Bertulis, A. Krotkus, *Appl. Phys. Lett.* **2007**, *91*, 051909
[21] K. Oe, H. Okamoto, *Jpn. J. Appl. Phys.* **1998**, *37*, L1283
[22] I. Vurgaftman, J. R. Meyer, L. R. Ram-Mohan, *J. Appl. Phys.* **2001**, *89*, 5815
[23] G. Pettinari, M. Capizzi, A. Polimeni, *Semicond. Sci. Technol.* **2015**, *30*, 094002
[24] G. Pettinari, A. Polimeni, M. Capizzi, H. Engelkamp, P. C. Christianen, J. C. Maan, A. Patane, T. Tiedje, *Phys. Status Solidi B* **2013**, *250*, 779
[25] M. Usman, C. A. Broderick, A. Lindsay, E. P. O'Reilly, *Phys. Rev. B* **2011**, *84*, 245202
[26] S. J. Sweeney, S. R. Jin, *J. Appl. Phys.* **2013**, *113*, 043110
[27] L. Wang, L. Zhang, L. Yue, D. Liang, X. Chen, Y. Li, P. Lu, J. Shao, S. Wang, *Crystals* **2017**, *7*, 63
[28] I. P. Marko, S. J. Sweeney, *IEEE J. Sel. Top. Quantum Electron.* **2017**, *23*, 1
[29] T. F. Kuech, S. E. Babcock, L. Mawst, *Applied Physics Reviews* **2016**, *3*, 040801
[30] F. Ishikawa, I. Buyanova, *Novel compound semiconductor nanowires: materials, devices, and applications*, CRC Press, **2017**
[31] Z. Zhou, D. F. Mendes, R. D. Richards, F. Bastiman, J. P. R. David, *Semicond. Sci. Technol.* **2015**, *30*, 094004
[32] C. J. Hunter, F. Bastiman, A. R. Mohmad, R. Richards, J. S. Ng, S. J. Sweeney, J. P. R. David, *IEEE Photonics Technol. Lett.* **2012**, *24*, 2191
[33] M. Masnadi-Shirazi, R. B. Lewis, V. Bahrami-Yekta, T. Tiedje, M. Chicoine, P. Servati, *J. Appl. Phys.* **2014**, *116*, 223506
[34] G. B. Lush, M. Melloch, M. Lundstrom, H. MacMillan, S. Asher, *J. Appl. Phys.* **1993**, *74*, 4694

[35] J. Tauc, *Amorphous and liquid semiconductors*, Springer Science & Business Media, London **2012**
[36] K. Kakuyama, S. Hasegawa, H. Nishinaka, M. Yoshimoto, *J. Appl. Phys.* **2019**, *126*, 045702
[37] C. Gogineni, N. A. Riordan, S. R. Johnson, X. Lu, T. Tiedje, *Appl. Phys. Lett.* **2013**, *103*, 041110
[38] Y. Liu, X. Yi, N. J. Bailey, Z. Zhou, T. B. O. Rockett, L. W. Lim, C. H. Tan, R. D. Richards, J. P. R. David, *Nat. Commun.* **2021**, *12*, 4784
[39] A. R. J. Marshall, C. H. Tan, M. J. Steer, J. P. R. David, *IEEE Photonics Technol. Lett.* **2009**, *21*, 866
[40] X. Yi, S. Xie, B. Liang, L. W. Lim, J. S. Cheong, M. C. Debnath, D. L. Huffaker, C. H. Tan, J. P. David, *Nat. Photonics* **2019**, *13*, 683
[41] R. R. King, D. C. Law, K. M. Edmondson, C. M. Fetzer, G. S. Kinsey, H. Yoon, R. A. Sherif, N. H. Karam, *Appl. Phys. Lett.* **2007**, *90*, 183516
[42] M. Green, E. Dunlop, J. Hohl-Ebinger, M. Yoshita, N. Kopidakis, X. Hao, *Prog. Photovoltaics* **2021**, *29*, 3
[43] T. Thomas, A. Mellor, N. P. Hylton, M. Führer, D. Alonso-Álvarez, A. Braun, N. J. Ekins-Daukes, J. P. R. David, S. J. Sweeney, *Semicond. Sci. Technol.* **2015**, *30*, 094010
[44] A. Zayan, M. Stevens, T. E. Vandervelde, *2016 IEEE 43rd Photovoltaic Specialists Conference (PVSC)* **2016**, 2839
[45] R. D. Richards, A. Mellor, F. Harun, J. S. Cheong, N. P. Hylton, T. Wilson, T. Thomas, J. S. Roberts, N. J. Ekins-Daukes, J. P. R. David, *Sol. Energy Mater. Sol. Cells* **2017**, *172*, 238
[46] H. Kim, K. Kim, Y. Guan, J. Lee, T. F. Kuech, L. J. Mawst, *Appl. Phys. Lett.* **2018**, *112*, 251105
[47] A. Muhammetgulyyev, O. G. Erbas, B. Kinaci, O. Donmez, Y. G. Celebi, A. Erol, *Semicond. Sci. Technol.* **2019**, *34*, 085001
[48] S. Hasegawa, K. Kakuyama, H. Nishinaka, M. Yoshimoto, *Jpn. J. Appl. Phys.* **2019**, *58*, 060907
[49] N. J. Ekins-Daukes, D. B. Bushnell, J. P. Connolly, K. W. J. Barnham, M. Mazzer, J. S. Roberts, G. Hill, R. Airey, *Phys. E* **2002**, *14*, 132
[50] R. D. Richards, T. B. O. Rockett, M. R. M. Nawawi, F. Harun, A. Mellor, T. Wilson, C. Christou, S. Chen, J. P. R. David, *Semicond. Sci. Technol.* **2018**, *33*, 094008
[51] M. A. Green, K. Emery, Y. Hishikawa, W. Warta, E. D. Dunlop, *Prog. Photovoltaics* **2011**, *19*, 565
[52] S. J. Sweeney, K. Hild, S. Jin, *2013 IEEE 39th Photovoltaic Specialists Conference (PVSC)* **2013**, 2474
[53] R. B. Lewis, D. A. Beaton, X. Lu, T. Tiedje, *J. Cryst. Growth* **2009**, *311*, 1872
[54] R. D. Richards, C. J. Hunter, F. Bastiman, A. R. Mohmad, J. P. R. David, *IET Optoelectron.* **2016**, *10*, 34
[55] P. K. Patil, E. Luna, T. Matsuda, K. Yamada, K. Kamiya, F. Ishikawa, S. Shimomura, *Nanotechnology* **2017**, *28*, 105702
[56] N. Hossain, I. P. Marko, S. R. Jin, K. Hild, S. J. Sweeney, R. B. Lewis, D. A. Beaton, T. Tiedje, *Appl. Phys. Lett.* **2012**, *100*, 051105
[57] X. Liu, L. Wang, X. Fang, T. Zhou, G. Xiang, B. Xiang, X. Chen, S. Hark, H. Liang, S. Wang, Z. Zhang, *Photonics Res.* **2019**, *7*, 508
[58] Y. Tominaga, K. Oe, M. Yoshimoto, *Appl. Phys. Express* **2010**, *3*, 062201
[59] T. Fuyuki, R. Yoshioka, K. Yoshida, M. Yoshimoto, *Appl. Phys. Lett.* **2013**, *103*, 202105

[60] X. Wu, W. Pan, Z. Zhang, Y. Li, C. Cao, J. Liu, L. Zhang, Y. Song, H. Ou, S. Wang, *ACS Photonics* **2017**, *4*, 1322
[61] P. Ludewig, N. Knaub, N. Hossain, S. Reinhard, L. Nattermann, I. P. Marko, S. R. Jin, K. Hild, S. Chatterjee, W. Stolz, S. J. Sweeney, K. Volz, *Appl. Phys. Lett.* **2013**, *102*, 242115
[62] T. Fuyuki, K. Yoshida, R. Yoshioka, M. Yoshimoto, *Appl. Phys. Express* **2014**, *7*, 082101
[63] R. Butkute, A. Geizutis, V. Paccebutas, B. Cechaviccius, V. Bukauskas, R. Kundrotas, P. Ludewig, K. Volz, A. Krotkus, *Electron. Lett* **2014**, *50*, 1155
[64] J. Glemža, V. Palenskis, A. Geižutis, B. Čechavičius, R. Butkutė, S. Pralgauskaitė, J. Matukas, *Materials* **2019**, *12*, 673
[65] Z. Zhang, L. Zhang, M. Zhang, S. Yao, P. Yu, X. Li, *Quantum Electron.* **2021**, *51*, 201
[66] M. Zhang, L. Zhang, Z. Zhang, P. Yu, S. Yao, *Electron. Mater. Lett.* **2021**, *17*, 181-187
[67] I. Marko, P. Ludewig, Z. Bushell, S. Jin, K. Hild, Z. Batool, S. Reinhard, L. Nattermann, W. Stolz, K. Volz, *J. Phys. D: Appl. Phys.* **2014**, *47*, 345103
[68] C. A. Broderick, P. E. Harnedy, E. P. O'Reilly, *IEEE J. Sel. Top. Quantum Electron.* **2015**, *21*, 287
[69] L. A. Samoska, *IEEE Trans. Terahertz Sci. Technol.* **2011**, *1*, 9
[70] N. M. Burford, M. O. El-Shenawee, *Opt. Eng.* **2017**, *56*, 010901
[71] R. N. Kini, C. P. Vaisakh, *Terahertz Emission Mechanisms in III–V Semiconductors: The Influence of Isoelectronic Dopants*, Springer, Singapore **2020**
[72] C. P. Vaisakh, A. Mascarenhas, R. N. Kini, *J. Appl. Phys.* **2015**, *118*, 165702
[73] K. Radhanpura, S. Hargreaves, R. A. Lewis, M. Henini, *Appl. Phys. Lett.* **2009**, *94*, 251115
[74] D. R. Bacon, J. Madéo, K. M. Dani, *J. Opt.* **2021**, *23*, 064001
[75] Z. Liliental-Weber, H. Cheng, S. Gupta, J. Whitaker, K. Nichols, F. Smith, *J. Electron. Mater.* **1993**, *22*, 1465
[76] J. M. Kim, Y. T. Lee, J. D. Song, J. H. Kim, *J. Cryst. Growth* **2004**, *265*, 8
[77] K. Bertulis, A. Krotkus, G. Aleksejenko, V. Pacebutas, R. Adomavicius, G. Molis, S. Marcinkevicius, *Appl. Phys. Lett.* **2006**, *88*, 201112
[78] V. Pačebutas, A. Bičiūnas, S. Balakauskas, A. Krotkus, G. Andriukaitis, D. Lorenc, A. Pugžlys, A. Baltuška, *Appl. Phys. Lett.* **2010**, *97*, 031111
[79] V. Pačebutas, A. Bičiūnas, K. Bertulis, A. Krotkus, *Electron. Lett* **2008**, *44*, 1154
[80] G. Molis, R. Adomavičius, A. Krotkus, K. Bertulis, L. Giniūnas, J. Pocius, R. Danielius, *Electron. Lett* **2007**, *43*, 190
[81] A. Arlauskas, P. Svidovsky, K. Bertulis, R. Adomavičius, A. Krotkus, *Appl. Phys. Express* **2012**, *5*, 022601
[82] V. Pačebutas, A. Urbanowicz, P. Cicėnas, S. Stanionytė, A. Bičiūnas, I. Nevinskas, A. Krotkus, *Semicond. Sci. Technol.* **2015**, *30*, 094012
[83] B. Heshmat, M. Masnadi-Shirazi, R. B. Lewis, J. Zhang, T. Tiedje, R. Gordon, T. E. Darcie, *Adv. Opt. Mater.* **2013**, *1*, 714
[84] C. A. Broderick, S. Mazzucato, H. Carrère, T. Amand, H. Makhloufi, A. Arnoult, C. Fontaine, O. Donmez, A. Erol, M. Usman, *Phys. Rev. B* **2014**, *90*, 195301
[85] S. Azaizia, A. Balocchi, S. Mazzucato, F. Cadiz, F. B. de le Salle, H. Lehec, D. Lagarde, A. Arnoult, T. Amend, C. Fontaine, H. Carrere, X. Marie, *Semicond. Sci. Technol.* **2018**, *33*, 114013
[86] H. Tong, X. Marie, M. Wu, *J. Appl. Phys.* **2012**, *112*, 063701

[87] B. Pursley, M. Luengo-Kovac, G. Vardar, R. S. Goldman, V. Sih, *Appl. Phys. Lett.* **2013**, *102*, 022420
[88] S. Mazzucato, T. T. Zhang, H. Carrère, D. Lagarde, P. Boonpeng, A. Arnoult, G. Lacoste, A. Balocchi, T. Amand, C. Fontaine, X. Marie, *Appl. Phys. Lett.* **2013**, *102*, 252107
[89] S. Tixier, M. Adamcyk, E. C. Young, J. H. Schmid, T. Tiedje, *J. Cryst. Growth* **2003**, *251*, 449
[90] R. D. Richards, F. Bastiman, C. J. Hunter, D. F. Mendes, A. R. Mohmad, J. S. Roberts, J. P. R. David, *J. Cryst. Growth* **2014**, *390*, 120
[91] T. B. O. Rockett, R. D. Richards, Y. Gu, F. Harun, Y. Liu, Z. Zhou, J. P. R. David, *J. Cryst. Growth* **2017**, *477*, 139
[92] T. Walther, R. D. Richards, F. Bastiman, *Cryst. Res. Technol.* **2015**, *50*, 38
[93] V. Bahrami-Yekta, T. Tiedje, M. Masnadi-Shirazi, *Semicond. Sci. Technol.* **2015**, *30*, 094007
[94] R. B. Lewis, M. Masnadi-Shirazi, T. Tiedje, *Appl. Phys. Lett.* **2012**, *101*, 082112
[95] M. Yoshimoto, S. Murata, A. Chayahara, Y. Horino, J. Saraie, K. Oe, *Jpn. J. Appl. Phys.* **2003**, *42*, L1235
[96] N. Riordan, C. Gogineni, S. Johnson, X. Lu, T. Tiedje, D. Ding, Y. Zhang, R. Fritz, K. Kolata, S. Chatterjee, K. Volz, S. Koch, *J. Mater. Sci.: Mater. Electron.* **2012**, 1-6
[97] R. Butkutė, V. Pačebutas, A. Krotkus, N. Knaub, K. Volz, *Lith. J. Phys.* **2014**, *54*, 125
[98] C. R. Tait, L. Yan, J. M. Millunchick, *J. Cryst. Growth* **2018**, *493*, 20
[99] A. J. Ptak, R. France, D. A. Beaton, K. Alberi, J. Simon, A. Mascarenhas, C. S. Jiang, *J. Cryst. Growth* **2012**, *338*, 107
[100] A. G. Norman, R. France, A. J. Ptak, *J. Vac. Sci. Technol., B: Microelectron. Nanometer Struct.-Process., Meas., Phenom.* **2011**, *29*, 03C121
[101] W. Pan, L. Wang, Y. Zhang, W. Lei, S. Wang, *Appl. Phys. Lett.* **2019**, *114*, 152102
[102] J. Puustinen, M. Wu, E. Luna, A. Schramm, P. Laukkanen, M. Laitinen, T. Sajavaara, M. Guina, *J. Appl. Phys.* **2013**, *114*, 243504
[103] C. Cornille, A. Arnoult, Q. Gravelier, C. Fontaine, *J. Appl. Phys.* **2019**, *126*, 093106
[104] H. Makhloufi, P. Boonpeng, S. Mazzucato, J. Nicolai, A. Arnoult, T. Hungria, G. Lacoste, C. Gatel, A. Ponchet, H. Carrere, X. Marie, C. Fontaine, *Nanoscale Res. Lett.* **2014**, *9*, 123
[105] W. Bennarndt, G. Boehm, M.-C. Amann, *J. Cryst. Growth* **2016**, *436*, 56
[106] X. Lu, D. A. Beaton, R. B. Lewis, T. Tiedje, M. B. Whitwick, *Appl. Phys. Lett.* **2008**, *92*, 192110
[107] J. Puustinen, J. Hilska, M. Guina, *J. Cryst. Growth* **2019**, *511*, 33
[108] R. Feenstra, J. Woodall, G. Pettit, *Phys. Rev. Lett.* **1993**, *71*, 1176
[109] R. Field III, J. Occena, T. Jen, M. Luengo-Kovac, B. Yarlagadda, V. Sih, C. Kurdak, R. Goldman, *APS March Meeting Abstracts* **2015**, *2015*, S14.014
[110] J. Steele, R. A. Lewis, J. Horvat, M. J. B. Nancarrow, M. Henini, D. Fan, Y. Mazur, M. Schmidbauer, M. Ware, S.-Q. Yu, *Sci. Rep.* **2016**, *6*, 1
[111] F. Bastiman, A. G. Cullis, J. P. R. David, S. J. Sweeney, *J. Cryst. Growth* **2012**, *341*, 19
[112] D. F. Reyes, F. Bastiman, C. J. Hunter, D. L. Sales, A. M. Sanchez, J. P. R. David, D. González, *Nanoscale Res. Lett.* **2014**, *9*, 1
[113] B. A. Carter, V. Caro, L. Yue, C. R. Tait, J. M. Millunchick, *J. Cryst. Growth* **2020**, *548*, 125815
[114] G. Vardar, S. Paleg, M. Warren, M. Kang, S. Jeon, R. Goldman, *Appl. Phys. Lett.* **2013**, *102*, 042106
[115] E. C. Young, S. Tixier, T. Tiedje, *J. Cryst. Growth* **2005**, *279*, 316

[116] J. A. Steele, J. Horvat, R. A. Lewis, M. Henini, D. Fan, Y. I. Mazur, V. G. Dorogan, P. C. Grant, S. Q. Yu, G. J. Salamo, *Nanoscale* **2015**, *7*, 20442
[117] J. A. Steele, R. A. Lewis, M. Henini, O. M. Lemine, D. Fan, Y. I. Mazur, V. G. Dorogan, P. C. Grant, S. Q. Yu, G. J. Salamo, *Opt. Express* **2014**, *22*, 11680
[118] C. R. Tait, L. Yan, J. M. Millunchick, *Appl. Phys. Lett.* **2017**, *111*, 042105
[119] C. R. Tait, J. M. Millunchick, *J. Appl. Phys.* **2016**, *119*, 215302
[120] G. V. Rodriguez, J. M. Millunchick, *J. Appl. Phys.* **2016**, *120*, 125310
[121] R. D. Richards, F. Harun, M. R. M. Nawawi, Y. Liu, T. B. O. Rockett, J. P. R. David, *J. Phys. D: Appl. Phys.* **2021**, *54*, 195102
[122] D. Fan, P. C. Grant, S.-Q. Yu, V. G. Dorogan, X. Hu, Z. Zeng, C. Li, M. E. Hawkridge, M. Benamara, Y. I. Mazur, *J. Vac. Sci. Technol., B: Microelectron. Nanometer Struct.--Process., Meas., Phenom.* **2013**, *31*, 03C105
[123] A. R. Mohmad, F. Bastiman, C. J. Hunter, F. Harun, D. F. Reyes, D. L. Sales, D. Gonzalez, R. D. Richards, J. P. R. David, B. Y. Majlis, *Semicond. Sci. Technol.* **2015**, *30*, 094018
[124] A. W. Wood, S. E. Babcock, J. Li, A. S. Brown, *J. Vac. Sci. Technol., A* **2015**, *33*, 031506
[125] M. A. Stevens, K. A. Grossklaus, J. H. McElearney, T. E. Vandervelde, *J. Electron. Mater.* **2019**, *48*, 3376
[126] P. C. Grant, D. S. Fan, A. Mosleh, S. Q. Yu, V. G. Dorogan, M. E. Hawkridge, Y. I. Mazur, M. Benamara, G. J. Salamo, S. R. Johnson, *J. Vac. Sci. Technol. B* **2014**, *32*, 02C119
[127] H. Kim, Y. X. Guan, S. E. Babcock, T. F. Kuech, L. J. Mawst, *J. Appl. Phys.* **2018**, *123*, 113102
[128] S. Mazzucato, P. Boonpeng, H. Carrere, D. Lagarde, A. Arnoult, G. Lacoste, T. Zhang, A. Balocchi, T. Amand, X. Marie, C. Fontaine, *Semicond. Sci. Technol.* **2013**, *28*, 022001
[129] A. R. Mohmad, F. Bastiman, C. J. Hunter, R. Richards, S. J. Sweeney, J. S. Ng, J. P. R. David, *Appl. Phys. Lett.* **2012**, *101*, 012106
[130] D. Sentosa, X. Tang, Z. Yin, S. J. Chua, *J. Cryst. Growth* **2007**, *307*, 229
[131] G. Mussler, J. M. Chauveau, A. Trampert, M. Ramsteiner, L. Däweritz, K. H. Ploog, *J. Cryst. Growth* **2004**, *267*, 60
[132] R. Butkute, G. Niaura, E. Pozingyte, B. Cechavicius, A. Selskis, M. Skapas, V. Karpus, A. Krotkus, *Nanoscale Res. Lett.* **2017**, *12*, 436
[133] M. Skapas, S. Stanionyte, T. Paulauskas, R. Butkute, *Phys. Status Solidi B* **2019**, *256*, 1800365
[134] J. Lagowski, M. Kaminska, J. Parsey Jr, H. Gatos, M. Lichtensteiger, *Appl. Phys. Lett.* **1982**, *41*, 1078
[135] G. Pettinari, A. Patané, A. Polimeni, M. Capizzi, X. Lu, T. Tiedje, *Appl. Phys. Lett.* **2012**, *101*, 222103
[136] G. Luo, S. Yang, G. R. Jenness, Z. Song, T. F. Kuech, D. Morgan, *NPG Asia Mater.* **2017**, *9*, e345
[137] S. Kamiyama, Y. Mori, Y. Takahashi, K. Ohnaka, *Appl. Phys. Lett.* **1991**, *58*, 2595
[138] L. F. DeChiaro, C. Sandroff, *IEEE Trans. Electron Devices* **1992**, *39*, 561
[139] V. N. Bessolov, M. V. Lebedev, Y. M. Shernyakov, B. V. Tsarenkov, *Mater. Sci. Eng., B* **1997**, *44*, 380
[140] R. Hakimi, M. Amann, *Semicond. Sci. Technol.* **1997**, *12*, 778

Robert Richards received his PhD in Electronic and Electrical Engineering from the University of Sheffield, UK, in 2014. He completed an EPSRC Doctoral Prize Fellowship and now holds a Royal Academy of Engineering Research Fellowship at the same university. He leads the dilute bismide MBE group, developing the growth of GaAsBi and related alloys, with a particular focus on the realization of high quality devices from these materials.

Nicholas Bailey gained an MEng in Microelectronics from the University of Sheffield in 2017. He is currently completing the final year of his doctoral degree at the University of Sheffield. His research is focused on the molecular beam epitaxy growth of dilute bismide semiconductors and understanding the effects that growth conditions have on their optoelectronic properties.

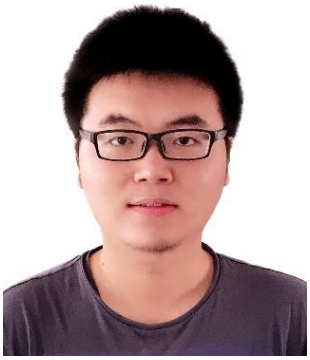

Yuchen Liu received B.Eng. and M.Sc. degrees in electrical engineering, semiconductor photonics and electronics from the University of Sheffield, UK in 2014 and 2016 respectively. He received his Ph.D. in electronic and electrical engineering from the University of Sheffield, UK in 2021 on the subject of the characterization of GaAsBi based semiconductors. Currently, he is working in the University of Sheffield on the project of quantum electro-optic detector technology. His research interests include MBE growth, avalanche photodiodes, and material characterization.

Thomas Rockett obtained an MPhys degree from Nottingham University in 2014, and a PhD from the University of Sheffield in 2019. Thomas previously worked at Ametek Land testing infrared thermometers for the steel and glass industry, and in the sensor systems group at the University of Sheffield where he researched thermal imaging applied to additive manufacturing. His research interests are near-infrared LEDs, photovoltaics, and temperature measurement.

Abdul Rahman Mohmad is a research fellow and senior lecturer at Universiti Kebangsaan Malaysia. He is also a Senior Member of the Institute of Electrical and Electronics Engineers. He completed his MEng and PhD in semiconductor materials and devices from the University of Sheffield, UK in 2008 and 2013, respectively. In 2016, he joined Prof. Chhowalla's group in Rutgers University, USA as a postdoctoral researcher for two years. His current research focuses on III-V semiconductors and two-dimensional transition metal dichalcogenides for optoelectronic and energy applications.